Precision Engineering 99 (2026) 246–257

Contents lists available at ScienceDirect

Precision Engineering

journal homepage: www.elsevier.com/locate/precision

Adaptive neural network fixed-time control of piezoelectric actuator for precision motion tracking

Yunzhi Zhang [a], Zhao Feng [b], Jie Ling [c], Chenyang Ding [a,*]

[a] College of Intelligent Robotics and Advanced Manufacturing, Fudan University, Shanghai, 200433, China
[b] School of Robotics, Wuhan University, Wuhan 430072, China
[c] College of Mechanical and Electrical Engineering, Nanjing University of Aeronautics and Astronautics, Nanjing 210016, China

ARTICLE INFO

Keywords:
Piezoelectric actuator
Fixed-time control
Neural network
Adaptive control
Precision motion

ABSTRACT

Piezoelectric actuators (PEAs) are critical in precision motion applications due to their high precision and fast response. Existing control methods for PEAs rely heavily on the accurate model integrated in the controllers to realize the precision motion tracking. However, complicated dynamics and inherent hysteresis nonlinearity bring challenges in modeling and identification. The accompanying model uncertainties bring difficulties for the rapid convergence of the tracking error and precision motion tracking of PEAs in the application. To overcome these limitations, this paper proposes an adaptive neural network fixed-time control (ANNFTC) scheme. The ANNFTC integrates the backstepping method and online neural network compensation, both designed according to the practical fixed-time stability. Unlike the fixed-time control (FTC) and related works, ANNFTC requires no prior knowledge of hysteresis while ensuring robustness to external disturbance and model uncertainties, including unmodeled dynamics and hysteresis nonlinearity. Rigorous proof of practical fixed-time convergence for the tracking error is provided, along with comprehensive experimental validation conducted on a PEA. The experimental campaign encompasses reference tracking across frequencies ranging from 1 to 10 Hz and peak-to-peak amplitudes from 1 to 9 μm, as well as hybrid-frequency sinusoidal tracking in the presence of input disturbances. Experimental results show that compared to other tested FTCs, ANNFTC achieves better tracking accuracy and more rapid convergence time of tracking error under different initial states, the existence of model uncertainties, and the external disturbance.

1. Introduction

Precision motion tracking has gained increasing significance with the rapid growth of micro/nano applications, such as semiconductor equipments [1], medical devices [2], aeronautical actuation systems [3], and related fields. Piezoelectric actuators (PEAs) are widely utilized in these precision motion systems due to their high precision, resolution, fast response, and compact structure [4]. However, the motion accuracy of PEAs is degraded by inherent nonlinearities (e.g., creep, hysteresis) [5] and other model uncertainties in controllers (e.g., unmodeled dynamics and parameter perturbation) [6,7].

For nonlinearities compensation of PEAs, several effective approa ches have been proposed for model-based feedforward controller design [7,8]. However, feedforward schemes alone are not robust to model uncertainties, as identified nominal models fail to accurately reflect the real system. In contrast, feedback control methods, which are more robust without requiring a precise mathematical model of the PEA, have been explored to improve motion accuracy [9,10]. Within feedback control strategies, tracking performance can be ensured by treating the nonlinearities as unknown disturbances [5]. Lyapunov-based techniques, such as backstepping control, can guarantee the stability and tracking accuracy of nonlinear systems like PEAs [11].

However, to the best of our knowledge, most of the feedback control on PEA's precision motion tracking focuses primarily on achieving asymptotic stability, which means achieving zero tracking error only after an infinite amount of time. This does not meet the practical requirements of engineering applications. From a practical perspective, the settling time is a critical performance metric for time-sensitive systems, as it characterizes the speed at which the system converges [12]. To address this limitation, finite-time control [13], fixed-time control (FTC) [14–16] and prescribed-time control (PTC) [17,18] have emerged as prominent approaches within the control community. In contrast to finite-time control, both FTC and PTC ensure convergence without dependence on the initial conditions. Compared with FTC, PTC offers a distinct advantage in that its settling time can be precisely

* Corresponding author.
E-mail address: dingcy@fudan.edu.cn (C. Ding).

https://doi.org/10.1016/j.precisioneng.2026.01.015
Received 10 October 2025; Received in revised form 20 December 2025; Accepted 13 January 2026
Available online 15 January 2026

preset, whereas that of FTC tends to be overestimated. Moreover, the settling time in FTC is not an independent tunable parameter, as it inherently depends on other controller design parameters. However, PTC often suffers from input saturation, higher online computational demands, and challenges in incorporating adaptive control mechanisms [13]. By comparison, although FTC only ensures that the convergence time remains below a predetermined upper bound, it generally exhibits simpler controller design, lower real-time computational requirements, and greater compatibility with adaptive control strategies, making it more amenable to practical engineering applications. FTC enables finite-time convergence of system dynamics regardless of the initial condition if the following inequality $\dot{V}(x) \leq -\alpha V^p(x) - \beta V^q(x)$ holds [19]. Nevertheless, when system uncertainty is considered, achieving fixed-time convergence becomes challenging because the uncertainty makes it difficult to satisfy the inequality conditions previously discussed [12]. To address this issue, [20] proposed the concept of practically fixed-time stability, which relaxes the conditions of the above FTC inequality.

Due to priority in practical use, FTC is integrated with sliding mode control (SMC) for the tracking control [21–23]. For the precision motion of the PEAs, [15] developed a local fixed-time SMC with an adaptive disturbance observer for a PEA system with unmodeled uncertainties. This controller demonstrates superior robustness and tracking accuracy compared to existing SMC. However, a limitation is that it requires explicit knowledge of the hysteresis part, $h(t)$, which complicates controller parameter tuning and design. [16] proposed a fast fixed-time adaptive SMC method that exhibits excellent dynamic tracking performance, steady-state behavior, and robustness to lumped disturbances. Nevertheless, this approach involves many adjustable parameters, requiring not only a system model that incorporates the explicit hysteresis part but also parameters for both the FTC and SMC. Meanwhile, SMC appears less suitable for PEA systems due to their rapid motion, significant model uncertainties, and lightly damped dynamics—factors that can induce control chattering and complicate SMC design. In summary, the aforementioned FTC methods for PEAs require sufficient prior knowledge of the system's dynamics and hysteresis nonlinearity. The implementation of this method entails increased controller complexity and poses subsequent challenges for parameter identification and tuning.

In cases where a system is entirely unknown or uncertain, neural networks (NN) perform online estimation of unknown nonlinear dynamics [24–26]. With respect to these circumstances, the FTC with NN compensation seems more suitable for realizing practically fixed-time stability to nonlinear systems like PEAs with disturbance and uncertainty. Several existing studies have investigated NN-based FTC for nonlinear systems [27–30]. However, the adaptive laws for NN weights proposed in [27–29] only ensure asymptotic stability. This limitation fails to theoretically guarantee simultaneous convergence of NN weight estimation errors and system state errors, often resulting in slower convergence rates and degraded tracking performance in the presence of transient disturbances. Although the adaptive law introduced in [30] incorporates a fixed-time convergence term, it utilizes a hyperbolic tangent (tanh) function whose argument depends on the product of the norm of the network basis function vector and the state error. This formulation is susceptible to saturation effects when either the error magnitude or the norm of the basis function vector is large, ultimately impairing convergence speed. Hence, a modified NN weights adaptive law with the fixed-time and rapid convergence property needs to be developed for PEAs.

Motivated by the aforementioned essential issues, a novel adaptive neural network fixed-time control (ANNFTC) scheme is developed in this work to enable high-precision and rapid convergence of tracking error of PEAs under the existence of external disturbance and model uncertainties, including: (1) complex hysteresis nonlinearity and (2) unmodeled dynamics. The main contributions of this paper are summarized below:

- A modified adaptive neural network control scheme with a novel NN weights update law is developed to realize the fixed-time convergence of tracking error. The only prior knowledge required for the controller is a standard second-order LTI model of the PEA, which is easy to identify and gain. A detailed theoretical proof of the controller design and practical fixed-time convergence is provided.
- Through an elaborate design, the proposed ANNFTC effectively handles the issues of nonlinearities, unmodeled dynamics, and external disturbance. For practical implementation, the state variables required by the control law are filtered with a stable filter, eliminating the need for a state observer and simplifying the control scheme. Detailed discussions on the proposed ANNFTC's performance are conducted via comprehensive experiments, along with comparisons to other FTCs, to illustrate the superiority of the proposed method.

The overall structure of the paper is outlined as follows. Section 2 introduces several essential lemmas needed in the controller design and the problem formulation. Section 3 gives the presentation of the proposed ANNFTC and its detailed practical fixed-time convergence proof. Section 4 provides a preliminary simulation of error convergence using ANNFTC, along with comparison results from the other controllers, including traditional FTC, the widely-used PID controller, and the finite-time control. Section 5 elaborates on the experiential setup and the closed-loop experiments with ANNFTC on the PEA, comparing the tracking performance and hysteresis compensation with the traditional FTC and the adaptive FTC with NN (AFTC) in [27]. Finally, Section 6 presents the conclusions.

2. Preliminaries and problem formulation

2.1. Preliminaries

This section firstly introduces some key lemmas related to fixed-time control, which are required in the proof process of the proposed method in this paper.

Lemma 1 ([27]). *Consider the nonlinear system as follows*

$$\dot{x}(t) = f(x(t)), x(0) = x_0. \tag{1}$$

If there exists a selected Lyapunov function $V(x)$ with some design constants, $\alpha, \beta > 0, p > 1, 0 < q < 1, 0 < \eta < \infty$ such that

$$\dot{V}(x) \leq -\alpha V^p(x) - \beta V^q(x) + \eta, \tag{2}$$

then with a constant $0 < \psi < 1$ introduced, the state of this system in Eq. (1) is practical fixed-time stable for any initial condition x_0 and the settling time T is estimated by

$$T \leq T_{max} = \frac{1}{\alpha\psi(p-1)} + \frac{1}{\beta\psi(1-q)}. \tag{3}$$

The residual set of the solution of the system $\dot{x} = f(x)$ is given by

$$x \in \left\{ V(x) \leq min \left\{ \left(\frac{\eta}{(1-\psi)\alpha} \right)^{1/p}, \left(\frac{\eta}{(1-\psi)\beta} \right)^{1/q} \right\} \right\}. \tag{4}$$

Lemma 2 (*Young's Inequality*). *For $a, b > 0, p > 1, 1/p + 1/q = 1$, the following inequality holds*

$$ab \leq \frac{a^p}{p} + \frac{b^q}{q}. \tag{5}$$

Lemma 3 (*Cauchy–Schwarz Inequality*). *: For $x, y \in \mathbb{R}^n$, the following inequality holds*

$$|x^\top y|^2 \leq x^\top x \cdot y^\top y. \tag{6}$$

Lemma 4 ([31]). *For real variables z and ζ, and any positive constants μ, η and ι, the following inequality is true:*

$$|z|^\mu |\zeta|^\eta \leq \frac{\mu}{\mu+\eta}\iota|z|^{\mu+\eta} + \frac{\eta}{\mu+\eta}\iota^{-\frac{\mu}{\eta}}|\zeta|^{\mu+\eta}. \tag{7}$$

Lemma 5 ([14]). *For $h > 0, x \geq 0, y \geq 0$, the following inequality holds*

$$x^h(y-x) \leq \frac{1}{1+h}(y^{1+h} - x^{1+h}). \tag{8}$$

Lemma 6 ([14]). *For $h > 1, x > 0, y \leq x, y \in \mathbb{R}$, it holds that*

$$(x-y)^h \geq y^h - x^h. \tag{9}$$

Lemma 7 ([32]). *For any real numbers $x_i, i = 1, \ldots, n$ and $0 < b < 1$, the following inequality holds:*

$$(|x_1| + \cdots + |x_n|)^b \leq |x_1|^b + \cdots + |x_n|^b. \tag{10}$$

Lemma 8 ([33]). *For all positive numbers $x_i, i = 1, 2, \ldots, n$, it holds*

$$\begin{aligned} &\sum_{i=1}^{n} x_i^{\gamma} \geq \Big(\sum_{i=1}^{n} x_i \Big)^{\gamma}, 0 < \gamma < 1, \\ &\sum_{i=1}^{n} x_i^{\gamma} \geq n^{1-\gamma} \Big(\sum_{i=1}^{n} x_i \Big)^{\gamma}, \gamma > 1. \end{aligned} \tag{11}$$

2.2. Problem formulation

Consider the following second-order system of a PEA to be controlled,

$$m\ddot{x} + c\dot{x} + kx = Tu + f, \tag{12}$$

where m, c, k are the equivalent mass, damping, and stiffness. x is the output displacement of the PEA, $\dot{x}$ and $\ddot{x}$ are the velocity and acceleration, respectively. u is the input signal to actuate the PEA and T is the electromechanical ratio, and f are the unknown disturbances which is caused by the model uncertainties in this paper.

Define $x_1 = x$, $x_2 = \dot{x}$, the system dynamic is reformulated by

$$\begin{cases} \dot{x}_1 = x_2, \\ \dot{x}_2 = -\dfrac{c}{m}x_2 - \dfrac{k}{m}x_1 + \dfrac{T}{m}u + \dfrac{1}{m}f \\ \quad = -a_2x_2 - a_1x_1 + bu + d. \end{cases} \tag{13}$$

The goal of this paper is to design an adaptive controller with fixed-time convergence for the aforementioned second-order system of a PEA.

3. Adaptive neural network fixed-time control

To realize the adaptive fixed-time control of the PEA system in Eq. (13), two error variables, denoted as $z_1 = x_1 - x_d, z_2 = x_2 - \nu$, where x_d is the reference signal, ν represents a virtual term, are introduced. Then, the tracking error dynamics are represented by

$$\begin{cases} \dot{z}_1 = \dot{x}_1 - \dot{x}_d = z_2 + \nu - \dot{x}_d, \\ \dot{z}_2 = \dot{x}_2 - \dot{\nu} = -a_2x_2 - a_1x_1 + bu + d - \dot{\nu}. \end{cases} \tag{14}$$

Next, use the backstepping method to deduce the control law, which can be divided into three steps as follows:

Step 1: Define Lyapunov function $V_1 = z_1^2/2$, the time derivative of V_1 is computed as

$$\dot{V}_1 = z_1\dot{z}_1 = z_1(z_2 + \nu - \dot{x}_d). \tag{15}$$

The virtual term ν is designed as

$$\begin{aligned} &\nu = -k_1|z_1|^{\alpha}\mathrm{sign}(z_1) - k_2|z_1|^{2\beta+1}\mathrm{sign}(z_1) + \dot{x}_d, \\ &0 < \alpha < 1, \beta \in \mathbb{N}^+. \end{aligned} \tag{16}$$

Then, substitute Eq. (16) into Eq. (15), one can obtain

$$\begin{aligned} \dot{V}_1 =& z_1 \Big(z_2 - k_1|z_1|^{\alpha}\mathrm{sign}(z_1) - k_2|z_1|^{2\beta+1}\mathrm{sign}(z_1) + \\ & \dot{x}_d - \dot{x}_d \Big) = -k_1|z_1|^{\alpha+1} - k_2|z_1|^{2(\beta+1)} + z_1z_2. \end{aligned} \tag{17}$$

Step 2: Define Lyapunov function $V_2 = z_2^2/2$, the time derivative of V_2 is computed as

$$\dot{V}_2 = z_2\dot{z}_2 = z_2 \left(-a_2x_2 - a_1x_1 + bu + d - \dot{\nu} \right). \tag{18}$$

Then, the control law is designed as

$$\begin{aligned} u = \frac{1}{b} \Big(& \dot{\nu} + a_2x_2 + a_1x_1 - z_1 - 1/2z_2 \\ & - k_3|z_2|^{\alpha}\mathrm{sign}(z_2) - k_4|z_2|^{2\beta+1}\mathrm{sign}(z_2) + \varphi_a \Big), \end{aligned} \tag{19}$$

where φ_a is the adaptive term to be determined. Substitute Eq. (19) into Eq. (18), one can obtain

$$\begin{aligned} \dot{V}_2 =& z_2 \Big(-a_2x_2 - a_1x_1 + \dot{\nu} + a_2x_2 + a_1x_1 - z_1 - \\ & 1/2z_2 - k_3|z_2|^{\alpha}\mathrm{sign}(z_2) - k_4|z_2|^{2\beta+1}\mathrm{sign}(z_2) + \varphi_a \\ & + d - \dot{\nu} \Big) = -z_1z_2 - \frac{1}{2}z_2^2 - k_3|z_2|^{\alpha+1} - k_4|z_2|^{2(\beta+1)} \\ & + z_2\varphi_a + z_2d. \end{aligned} \tag{20}$$

Then, add Eqs. (17) and (20), one can obtain

$$\begin{aligned} \dot{V}_1 + \dot{V}_2 =& -k_1|z_1|^{\alpha+1} - k_2|z_1|^{2(\beta+1)} - k_3|z_2|^{\alpha+1} - \\ & k_4|z_2|^{2(\beta+1)} - \frac{1}{2}z_2^2 + z_2\varphi_a + z_2d. \end{aligned} \tag{21}$$

Step 3: Here, the NN-based adaptive control law is to be designed. Supposing the number n of the node is chosen large enough, the disturbance d in Eq. (13) is calculated as

$$d = f(X) = W^{\top}\psi(X) + \epsilon, |\epsilon| \leq \bar{\epsilon}, \tag{22}$$

and make

$$\theta = W^{\top}W, \tilde{\theta} = \theta - \hat{\theta}. \tag{23}$$

Theorem 1. *For the system in Eq. (13), if the adaptive law is given as*

$$\begin{aligned} \varphi_a =& -\frac{1}{2\mu^2}z_2\psi(X)^{\top}\psi(X)\hat{\theta}, \\ \dot{\hat{\theta}} =& \gamma \left(\frac{1}{2\mu^2}z_2^2\psi(X)^{\top}\psi(X) - 2\sigma_1\hat{\theta} - \sigma_2\hat{\theta}^{2\beta+1} \right), \\ \hat{\theta} =& \begin{cases} \int \dot{\hat{\theta}}dt, & \text{if } \hat{\theta} \geq 0 \\ 0, & \text{if } \hat{\theta} < 0, \end{cases} \end{aligned} \tag{24}$$

and the control law is Eq. (19), the practical fixed-time stability can be achieved. The constraints of the $\hat{\theta}$ here is used to ensure the value of $\hat{\theta}$ is nonnegative, which is crucial for the subsequent proof.

Proof. Substitute Eq. (24) into Eq. (21), one can obtain

$$\begin{aligned} \dot{V}_1 + \dot{V}_2 =& -k_1|z_1|^{\alpha+1} - k_2|z_1|^{2(\beta+1)} - k_3|z_2|^{\alpha+1} + \\ & z_2\varphi_a + z_2d = -k_1|z_1|^{\alpha+1} - k_2|z_1|^{2(\beta+1)} - \\ & k_3|z_2|^{\alpha+1} - k_4|z_2|^{2(\beta+1)} - \frac{1}{2}z_2^2 - \\ & \frac{1}{2\mu^2}z_2^2\psi(X)^{\top}\psi(X)(\theta - \tilde{\theta}) + \\ & z_2(W^{\top}\psi(X) + \epsilon). \end{aligned} \tag{25}$$

Another Lyapunov function is designed as

$$V_3 = \frac{1}{2\gamma}\tilde{\theta}^2. \tag{26}$$

Applying Eq. (24), the differentiation of V_3 is

$$\begin{aligned} \dot{V}_3 =& -\frac{1}{\gamma}\tilde{\theta}\dot{\hat{\theta}} = -\tilde{\theta} \left(\frac{1}{2\mu^2}z_2^2\psi(X)^{\top}\psi(X) - 2\sigma_1\hat{\theta} - \sigma_2\hat{\theta}^{2\beta+1} \right) \\ =& -\frac{1}{2\mu^2}z_2^2\psi(X)^{\top}\psi(X)\tilde{\theta} + 2\sigma_1\tilde{\theta}\hat{\theta} + \sigma_2\tilde{\theta}\hat{\theta}^{2\beta+1}. \end{aligned} \tag{27}$$

Then, add Eqs. (25) and (27), one can obtain

$$\begin{aligned}\dot{V}_1+\dot{V}_2+\dot{V}_3=&-k_1|z_1|^{\alpha+1}-k_2|z_1|^{2(\beta+1)}-k_3|z_2|^{\alpha+1}-\\&k_4|z_2|^{2(\beta+1)}-\frac{1}{2}z_2^2-\frac{1}{2\mu^2}z_2^2\psi(X)^{\top}\psi(X)\\&(\theta-\tilde{\theta})+z_2(W^{\top}\psi(X)+\epsilon)-\\&\frac{1}{2\mu^2}z_2^2\psi(X)^{\top}\psi(X)\tilde{\theta}+2\sigma_1\tilde{\theta}\hat{\theta}+\sigma_2\tilde{\theta}\hat{\theta}^{2\beta+1}\\=&-k_1|z_1|^{\alpha+1}-k_2|z_1|^{2(\beta+1)}-k_3|z_2|^{\alpha+1}-\\&k_4|z_2|^{2(\beta+1)}-\frac{1}{2}z_2^2-\frac{1}{2\mu^2}z_2^2\psi(X)^{\top}\psi(X)\theta+\\&\underbrace{z_2W^{\top}\psi(X)}_{\text{Term 1}}+\underbrace{z_2\epsilon}_{\text{Term 2}}+\underbrace{2\sigma_1\tilde{\theta}\hat{\theta}}_{\text{Term 3}}+\underbrace{\sigma_2\tilde{\theta}\hat{\theta}^{2\beta+1}}_{\text{Term 4}}.\end{aligned}\tag{28}$$

(1) Term 1: The following inequality is obtained according to Lemmas 2 and 3

$$\begin{aligned}z_2W^{\top}\psi(X)\leq&\frac{1}{2\mu^2}(z_2W^{\top}\psi(X))^{\top}z_2W^{\top}\psi(X)+\frac{\mu^2}{2}\\=&\frac{1}{2\mu^2}z_2^2(W^{\top}\psi(X))^2+\frac{\mu^2}{2}\\\leq&\frac{1}{2\mu^2}z_2^2\left(\underbrace{W^{\top}W}_{\theta}\cdot\psi(X)^{\top}\psi(X)\right)+\frac{\mu^2}{2}\\=&\frac{1}{2\mu^2}z_2^2\theta\psi(X)^{\top}\psi(X)+\frac{\mu^2}{2}.\end{aligned}\tag{29}$$

(2) Term 2: Use the Lemma 2, the following inequality is obtained

$$z_2\epsilon\leq\frac{1}{2}z_2^2+\frac{1}{2}\bar{\epsilon}^2.\tag{30}$$

(3) Term 3: Firstly, according to Eq. (24) and Lemma 2, one can obtain

$$2\tilde{\theta}\hat{\theta}=2\tilde{\theta}(\theta-\tilde{\theta})=-2\tilde{\theta}^2+2\tilde{\theta}\theta\leq-2\tilde{\theta}^2+\tilde{\theta}^2+\theta^2=-\tilde{\theta}^2+\theta^2.\tag{31}$$

Make that

$$z=\tilde{\theta}^2,\zeta=1,\mu=p,\eta=1-p,\iota=\frac{1}{p},0<p=\frac{\alpha+1}{2}<1.\tag{32}$$

Then, according to Lemma 4, the following inequality holds

$$\begin{aligned}&(\tilde{\theta}^2)^{\frac{\alpha+1}{2}}\leq\tilde{\theta}^2+(1-p)p^{\frac{p}{1-p}}=\tilde{\theta}^2+\frac{1-\alpha}{2}\left(\frac{1+\alpha}{2}\right)^{\frac{1+\alpha}{1-\alpha}}\\&-\tilde{\theta}^2\leq-|\tilde{\theta}|^{\alpha+1}+\frac{1-\alpha}{2}\left(\frac{1+\alpha}{2}\right)^{\frac{1+\alpha}{1-\alpha}}.\end{aligned}\tag{33}$$

Finally, combine the inequalities in Eqs. (31) and (33), the following inequality holds

$$2\sigma_1\tilde{\theta}\hat{\theta}\leq-\sigma_1|\tilde{\theta}|^{\alpha+1}+\frac{\sigma_1(1-\alpha)}{2}\left(\frac{1+\alpha}{2}\right)^{\frac{1+\alpha}{1-\alpha}}+\sigma_1\theta^2.\tag{34}$$

(4) Term 4: According to Eqs. (22) and (24), $\hat{\theta}\geq0,\theta\geq0$ and $\tilde{\theta}\leq\theta$. Hence, it can be obtained with Lemmas 5 and 6

$$\begin{aligned}\tilde{\theta}\hat{\theta}^{2\beta+1}=&(\theta-\hat{\theta})\hat{\theta}^{2\beta+1}\leq\frac{1}{2(1+\beta)}(\theta^{2(\beta+1)}-\hat{\theta}^{2(\beta+1)})\\=&\frac{1}{2(1+\beta)}(\theta^{2(\beta+1)}-(\theta-\tilde{\theta})^{2(\beta+1)})\\\leq&\frac{1}{2(1+\beta)}\left(\theta^{2(\beta+1)}-(\tilde{\theta}^{2(\beta+1)}-\theta^{2(\beta+1)})\right)\\=&-\frac{1}{2(1+\beta)}|\tilde{\theta}|^{2(\beta+1)}+\frac{1}{1+\beta}\theta^{2(\beta+1)}.\end{aligned}\tag{35}$$

Therefore,

$$\sigma_2\tilde{\theta}\hat{\theta}^{2\beta+1}\leq-\frac{\sigma_2}{2(1+\beta)}|\tilde{\theta}|^{2(\beta+1)}+\frac{\sigma_2}{1+\beta}\theta^{2(\beta+1)}.\tag{36}$$

Finally, combine the Eq. (28) and the inequalities in (29), (30), (34) and (36), the following inequality holds

$$\begin{aligned}\dot{V}_1+\dot{V}_2+\dot{V}_3\leq&-k_1|z_1|^{\alpha+1}-k_2|z_1|^{2(\beta+1)}\\&-k_3|z_2|^{\alpha+1}-k_4|z_2|^{2(\beta+1)}+\frac{\mu^2}{2}+\frac{1}{2}\bar{\epsilon}^2-\\&\sigma_1|\tilde{\theta}|^{\alpha+1}+\frac{\sigma_1(1-\alpha)}{2}\left(\frac{1+\alpha}{2}\right)^{\frac{1+\alpha}{1-\alpha}}+\sigma_1\theta^2\\&-\frac{\sigma_2}{2(1+\beta)}|\tilde{\theta}|^{2(\beta+1)}+\frac{\sigma_2}{1+\beta}\theta^{2(\beta+1)}.\end{aligned}\tag{37}$$

Write the positive numbers in the Eq. (37) as C, one can obtain

$$\begin{aligned}\dot{V}_1+\dot{V}_2+\dot{V}_3\leq&-k_1|z_1|^{\alpha+1}-k_2|z_1|^{2(\beta+1)}-k_3|z_2|^{\alpha+1}-\\&k_4|z_2|^{2(\beta+1)}-\sigma_1|\tilde{\theta}|^{\alpha+1}-\frac{\sigma_2}{2(1+\beta)}|\tilde{\theta}|^{2(\beta+1)}+\\&\frac{\mu^2}{2}+\frac{1}{2}\bar{\epsilon}^2+\frac{\sigma_1(1-\alpha)}{2}\left(\frac{1+\alpha}{2}\right)^{\frac{1+\alpha}{1-\alpha}}+\\&\sigma_1\theta^2+\frac{\sigma_2}{1+\beta}\theta^{2(\beta+1)}\\=&-k_1|z_1|^{\alpha+1}-k_2|z_1|^{2(\beta+1)}-k_3|z_2|^{\alpha+1}-\\&k_4|z_2|^{2(\beta+1)}-\sigma_1|\tilde{\theta}|^{\alpha+1}-\frac{\sigma_2}{2(1+\beta)}|\tilde{\theta}|^{2(\beta+1)}\\&+C.\end{aligned}\tag{38}$$

Then, with $V=V_1+V_2+V_3$, it holds

$$\begin{aligned}\dot{V}\leq&-2^{\frac{\alpha+1}{2}}k_1\left(\frac{1}{2}z_1^2\right)^{\frac{\alpha+1}{2}}-2^{\frac{\alpha+1}{2}}k_3\left(\frac{1}{2}z_2^2\right)^{\frac{\alpha+1}{2}}-\\&(2\gamma)^{\frac{\alpha+1}{2}}\sigma_1\left(\frac{1}{2\gamma}\tilde{\theta}^2\right)^{\frac{\alpha+1}{2}}-2^{\beta+1}k_2\left(\frac{1}{2}z_1^2\right)^{\beta+1}-\\&2^{\beta+1}k_4\left(\frac{1}{2}z_2^2\right)^{\beta+1}-\frac{(2\gamma)^{\beta+1}\sigma_2}{2(1+\beta)}\left(\frac{1}{2\gamma}\tilde{\theta}^2\right)^{\beta+1}+C.\end{aligned}\tag{39}$$

Define the following variables as

$$\begin{aligned}\rho_1=&\min\left\{2^{\frac{\alpha+1}{2}}k_1,2^{\frac{\alpha+1}{2}}k_3,(2\gamma)^{\frac{\alpha+1}{2}}\sigma_1\right\},\\\rho_2=&\min\left\{2^{\beta+1}k_2,2^{\beta+1}k_4,\frac{(2\gamma)^{\beta+1}\sigma_2}{2(1+\beta)}\right\}.\end{aligned}\tag{40}$$

According to Lemma 7, it holds

$$\begin{aligned}&\rho_1(V_1+V_2+V_3)^{\frac{\alpha+1}{2}}\leq\rho_1V_1^{\frac{\alpha+1}{2}}+\rho_1V_2^{\frac{\alpha+1}{2}}+\rho_1V_3^{\frac{\alpha+1}{2}}\\&\leq2^{\frac{\alpha+1}{2}}k_1\left(\frac{1}{2}z_1^2\right)^{\frac{\alpha+1}{2}}+2^{\frac{\alpha+1}{2}}k_3\left(\frac{1}{2}z_2^2\right)^{\frac{\alpha+1}{2}}+\\&(2\gamma)^{\frac{\alpha+1}{2}}\sigma_1\left(\frac{1}{2\gamma}\tilde{\theta}^2\right)^{\frac{\alpha+1}{2}}\\&\rightarrow-\rho_1V^{\frac{\alpha+1}{2}}\geq-2^{\frac{\alpha+1}{2}}k_1\left(\frac{1}{2}z_1^2\right)^{\frac{\alpha+1}{2}}-\\&2^{\frac{\alpha+1}{2}}k_3\left(\frac{1}{2}z_2^2\right)^{\frac{\alpha+1}{2}}-(2\gamma)^{\frac{\alpha+1}{2}}\sigma_1\left(\frac{1}{2\gamma}\tilde{\theta}^2\right)^{\frac{\alpha+1}{2}}.\end{aligned}\tag{41}$$

If $n=3$, according to Lemma 8, it holds

$$\begin{aligned}&\rho_23^{-\beta}(V_1+V_2+V_3)^{\beta+1}\leq\rho_2V_1^{\beta+1}+\rho_2V_2^{\beta+1}+\rho_2V_3^{\beta+1}\\&\leq2^{\beta+1}k_2\left(\frac{1}{2}z_1^2\right)^{\beta+1}+2^{\beta+1}k_4\left(\frac{1}{2}z_4^2\right)^{\beta+1}+\\&\frac{(2\gamma)^{\beta+1}\sigma_2}{2(1+\beta)}\left(\frac{1}{2\gamma}\tilde{\theta}^2\right)^{\beta+1}\\&\rightarrow-\rho_23^{-\beta}V^{\beta+1}\geq-2^{\beta+1}k_2\left(\frac{1}{2}z_1^2\right)^{\beta+1}-\\&2^{\beta+1}k_4\left(\frac{1}{2}z_4^2\right)^{\beta+1}-\frac{(2\gamma)^{\beta+1}\sigma_2}{2(1+\beta)}\left(\frac{1}{2\gamma}\tilde{\theta}^2\right)^{\beta+1}.\end{aligned}\tag{42}$$

Finally, combine the inequalities in (39), (41) and (42), one can obtain

$$\dot{V}\leq-\rho_1V^{\frac{\alpha+1}{2}}-\rho_23^{-\beta}V^{\beta+1}+C,0<\alpha<1,\beta\in\mathbb{N}^+.\tag{43}$$

Thus, Theorem 1 is proved and the practical fixed-time stability is achieved.

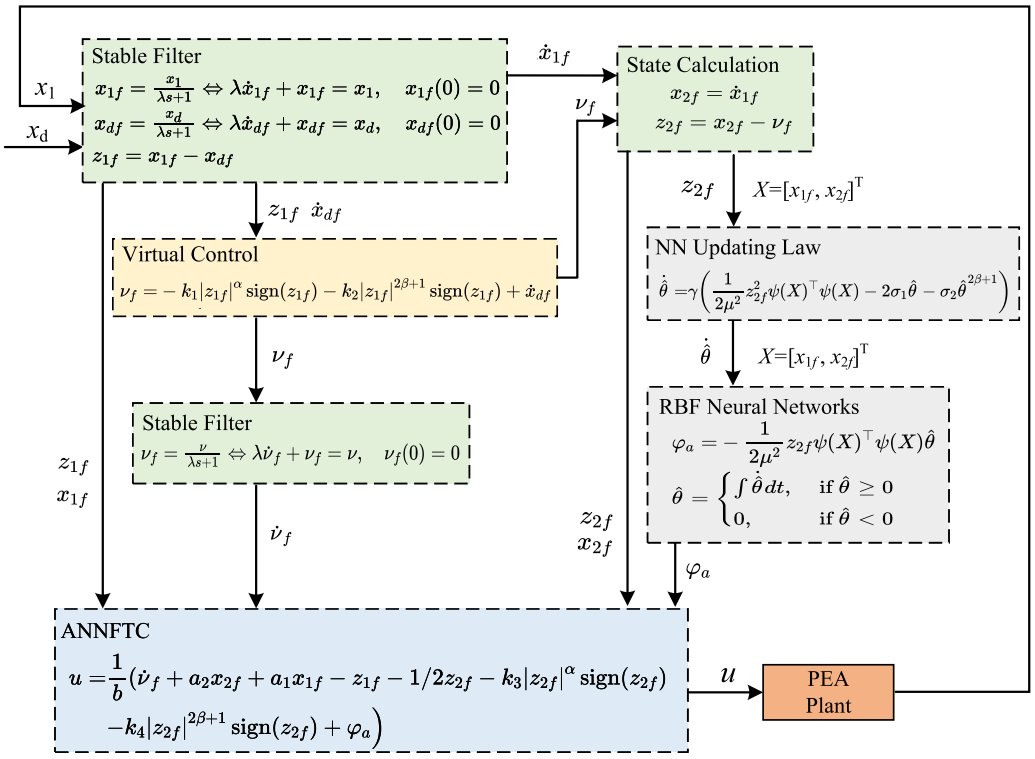

Fig. 1. The control block diagram of the proposed ANNFTC.

According to the aforementioned controller design, the overall control law of ANNFTC is:

$$\begin{aligned} u =& \frac{1}{b}\Big(\dot{\nu} + a_2 x_2 + a_1 x_1 - z_1 - 1/2 z_2 - k_3|z_2|^{\alpha}\text{sign}(z_2) \\ & - k_4|z_2|^{2\beta+1}\text{sign}(z_2) + \varphi_a\Big), \\ \nu =& -k_1|z_1|^{\alpha}\text{sign}(z_1) - k_2|z_1|^{2\beta+1}\text{sign}(z_1) + \dot{x}_d, \\ & 0 < \alpha < 1, \beta \in \mathbb{N}^+, \\ \varphi_a =& -\frac{1}{2\mu^2} z_2 \psi(X)^{\top}\psi(X)\hat{\theta}, \\ \dot{\hat{\theta}} =& \gamma\left(\frac{1}{2\mu^2} z_2^2 \psi(X)^{\top}\psi(X) - 2\sigma_1\hat{\theta} - \sigma_2\hat{\theta}^{2\beta+1}\right). \end{aligned} \tag{44}$$

From Eq. (44), it can be found that the derivatives of the intermediate variables and state variables are introduced. However, in practical applications, the differentiation process amplifies measurement noise and exists singularity issue in the differentiation of sign function shown in Eq. (44), potentially compromising system stability. Hence, in practical use, by applying a stable filter ($1 / (\lambda s+1)$) to the variables ν, x_1, and x_d, filtered variables are introduced as:

$$\begin{aligned} \nu_f =& \frac{\nu}{\lambda s+1} \Leftrightarrow \lambda \dot{\nu}_f + \nu_f = \nu \rightarrow \\ & \dot{\nu}_f = \frac{\nu - \nu_f}{\lambda}, \quad \nu_f(0) = 0, \end{aligned} \tag{45}$$

$$\begin{aligned} x_{1f} =& \frac{x_1}{\lambda s+1} \Leftrightarrow \lambda \dot{x}_{1f} + x_{1f} = x_1 \rightarrow \\ & \dot{x}_{1f} = \frac{x_1 - x_{1f}}{\lambda}, \quad x_{1f}(0) = 0, \end{aligned} \tag{46}$$

$$\begin{aligned} x_{df} =& \frac{x_d}{\lambda s+1} \Leftrightarrow \lambda \dot{x}_{df} + x_{df} = x_d \rightarrow \\ & \dot{x}_{df} = \frac{x_d - x_{df}}{\lambda}, \quad x_{df}(0) = 0, \end{aligned} \tag{47}$$

where $\lambda > 0$ is a filter parameter which is designed to guarantee that the cutoff frequency is much higher than the frequency of the tracking signal so that the filter error is neglected. Furthermore, $x_{2f} = \dot{x}_{1f}$, $z_{1f} = x_{1f} - x_{df}$, $z_{2f} = x_{2f} - \nu_f$.

Replace the filtered variables in Eq. (44) with Eqs. (45)–(47), the final control force applied to the PEA system is as follows:

$$\begin{aligned} u =& \frac{1}{b}\Big(\dot{\nu}_f + a_2 x_{2f} + a_1 x_{1f} - z_{1f} - 1/2 z_{2f} - \\ & k_3|z_{2f}|^{\alpha}\text{sign}(z_{2f}) - k_4|z_{2f}|^{2\beta+1}\text{sign}(z_{2f}) + \varphi_a\Big), \\ \nu_f =& -k_1|z_{1f}|^{\alpha}\text{sign}(z_{1f}) - k_2|z_{1f}|^{2\beta+1}\text{sign}(z_{1f}) + \dot{x}_{df}, \\ & 0 < \alpha < 1, \beta \in \mathbb{N}^+, \\ \varphi_a =& -\frac{1}{2\mu^2} z_{2f} \psi(X)^{\top}\psi(X)\hat{\theta}, X_f = [x_{1f}, x_{2f}], \\ \dot{\hat{\theta}} =& \gamma\left(\frac{1}{2\mu^2} z_{2f}^2 \psi(X)^{\top}\psi(X) - 2\sigma_1\hat{\theta} - \sigma_2\hat{\theta}^{2\beta+1}\right). \end{aligned} \tag{48}$$

The overall control scheme is shown in Fig. 1.

4. Preliminary simulation of error dynamics

A simple system shown in Eq. (49) is used to test the convergence of error with different controllers, including: the PID, FTC, Finite-time control and the proposed ANNFTC

$$\dot{x} = u + d, e = x - x_d, \tag{49}$$

where x is the state variable, u is the input and d is the disturbance. x_d is the desired state and e is the tracking error. Then, the derivative of the error can be obtained:

$$\dot{e} = u + d. \tag{50}$$

To control the system in Eq. (49), the control laws of the controllers are listed as:

(1) PID

$$\begin{aligned} u =& -k_p e - k_i \int e dt - k_d \dot{e}, \\ \dot{e} =& -k_p e - k_i \int e dt - k_d \dot{e} + d. \end{aligned} \tag{51}$$

(2) FTC:

$$u = -k_1|e|^{\alpha}\text{sign}(e) - k_2|e|^{2\beta+1}\text{sign}(e). \tag{52}$$

(3) Finite-time control:

$$u = -k_1|e|^{\alpha}\text{sign}(e) - k_2 e. \tag{53}$$

(4) ANNFTC:

$$\begin{aligned} u &= -\frac{e}{2} - k_1|e|^{\alpha}\text{sign}(e) - k_2|e|^{2\beta+1}\text{sign}(e) + \varphi_a, \\ \varphi_a &= -\frac{1}{2\mu^2} e\psi(X)^{\top}\psi(X)\hat{\theta}, \\ \dot{\hat{\theta}} &= \gamma\left(\frac{1}{2\mu^2} e^2\psi(X)^{\top}\psi(X) - 2\sigma_1\hat{\theta} - \sigma_2\hat{\theta}^{2\beta+1}\right). \end{aligned} \tag{54}$$

This section aims to validate the accuracy and effectiveness of the proposed ANNFTC by testing two scenarios: the absence of disturbances and the presence of disturbances. Firstly, the parameters without disturbances are set as follows:

$$\begin{aligned} &\text{(1) PID:} && k_p = 10;\ k_d = 1;\ k_i = 0, \\ &\text{(2) FTC:} && k_1 = 1;\ k_2 = 1;\ \alpha = 0.1;\ \beta = 1, \\ &\text{(3) Finite-time control:} && k_1 = 5;\ k_2 = 1;\ \alpha = 0.1, \\ &\text{(4) ANNFTC:} && k_1 = 1;\ k_2 = 1;\ \alpha = 0.1;\ \beta = 1; \\ & && \mu = 1; \gamma = 10;\ \sigma_1 = 1;\ \sigma_2 = 1, \end{aligned} \tag{55}$$

According to the parameters in Eq. (55) and the maximum setting time calculation which is shown in Eq. (3), the maximum setting time $T_{\max} = 2.0198$. The detailed error convergence and dynamics in this case are shown in Fig. 2. It is evident that, compared to the PID and Finite-time control, both FTC and ANNFTC achieve fixed-time error convergence, with the settling time controllable within the maximum convergence time T_{max}, calculated using Eq. (3). In this case, different initial error states are also considered to evaluate the initial-independence priority of the fixed-time convergence for both the FTC and ANNFTC. As shown clearly in Fig. 2, with three different initial error values (10-20-40), both FTC and ANNFTC can achieve fixed-time error convergence within the maximum convergence time T_{max}. In contrast, the settling time of Finite-time control increases with the rise of initial error values. This further verifies the rationality and superiority of the FTC and ANNFTC designed in this paper. Meanwhile, with the assistance of the neural network, ANNFTC demonstrates a faster convergence speed than FTC, even in the absence of disturbances.

Next, consider the case with disturbances. The parameters in this case are set with disturbance $d = 1 \cdot cos(2\pi \cdot 1 \cdot t)$:

$$\begin{aligned} &\text{(1) PID: } k_p = 10; k_d = 1; k_i = 0, \\ &\text{(2) FTC: } k_1 = 1; k_2 = 1; \alpha = 0.1; \beta = 1 \\ &\text{(3) ANNFTC-1: } k_1 = 1; k_2 = 1; \alpha = 0.1; \beta = 1; \\ &\qquad \mu = 1; \gamma = 10; \sigma_1 = \sigma_2 = 1, \\ &\text{(4) ANNFTC-2: } k_1 = 1; k_2 = 1; \alpha = 0.1; \beta = 1; \\ &\qquad \mu = 1; \gamma = 10; \sigma_1 = \sigma_2 = 10^{-6}. \end{aligned} \tag{56}$$

The detailed error convergence and dynamics in this case are shown in Fig. 3. It can be found that with the help of neural network compensation, the ANNFTC shows better convergence speed and smaller error than FTC and PID under the disturbance. Meanwhile, smaller value of σ_1 and σ_2 will help accelerate the convergence speed and tracking accuracy, which can serve as the parameter tuning method of ANNFTC.

5. Experimental evaluation

5.1. Experimental platform

The experimental evaluation was conducted on a custom-built platform incorporating a piezoelectric stack actuator (PEA) (Fig. 4(a-b)) to validate the effectiveness of the proposed ANNFTC. A piezoelectric stack (NAC2015, Harbin Chip Technology Co., Ltd) with a 12 μ m stroke and a maximum driving voltage of 100 V was used for actuation. The control system is based on an xPC Target real-time platform, consisting of a host PC, a target PC, a PCI-6259 motion acquisition card, and an interface board. Control signals (0–10 V) are generated in real time via the 16-bit digital-to-analog converter of the data output module in the xPC Target environment. A custom-built power amplifier with a fixed gain of 30 amplifies the control signal to provide the driving voltage for the PEA. Displacement of the PEA is measured using a capacitive displacement sensor (E09.Cap, Harbin Core Tomorrow Science & Technology Co., Ltd).

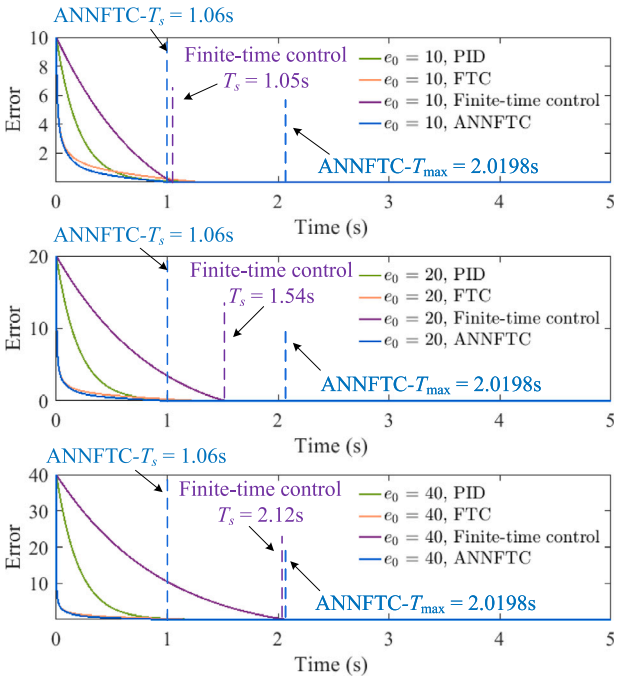

Fig. 2. Error convergence of the four controllers with different initial states and without disturbances.

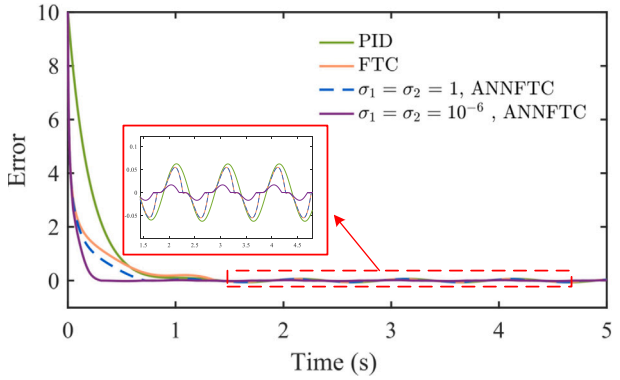

Fig. 3. Error convergence with different parameters for disturbance compensation.

5.2. System identification

A high-amplitude (100 V) step response test is conducted to identify the nominal model $G(s)$ in Eq. (12). A second-order LTI model is obtained using the System Identification Toolbox in MATLAB as,

$$G(s) = \frac{2.63 \times 10^6}{s^2 + 5300s + 2.534 \times 10^7}. \tag{57}$$

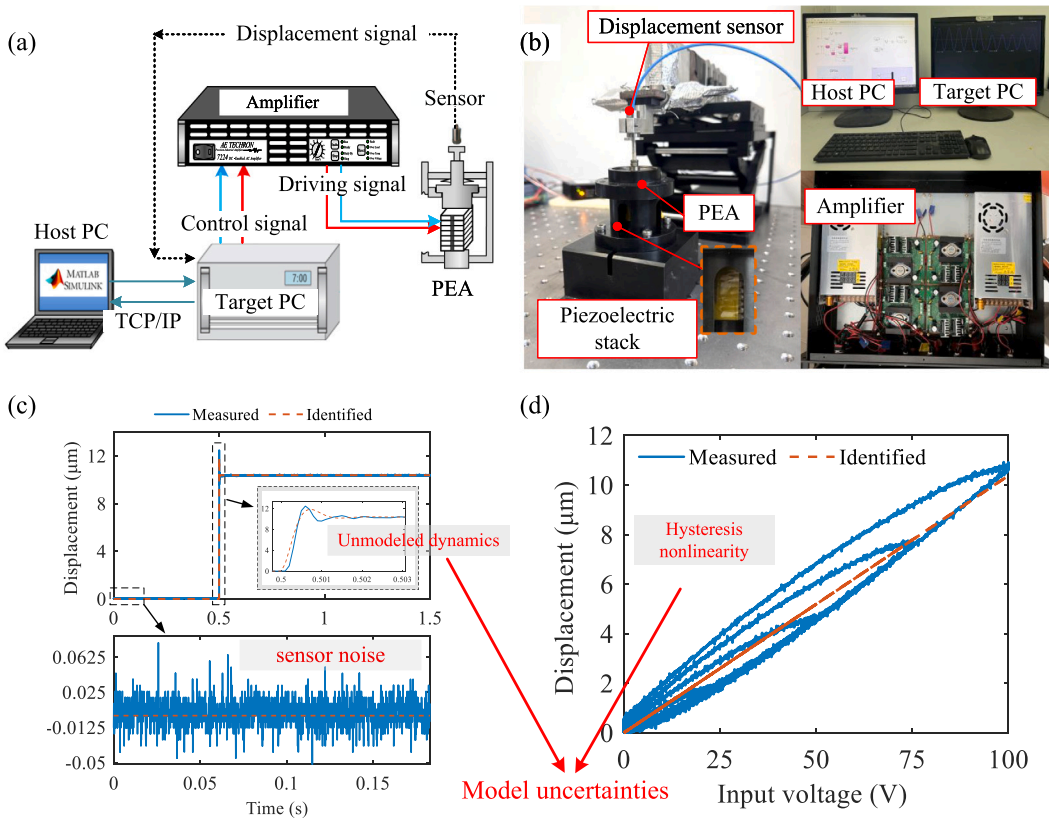

Fig. 4. Experimental setup and system identification results. (a) Block diagram of signal flow. (b) Experimental system. (c) Identification results with a step response and the evaluation of sensor noise. (d) Tested hysteresis nonlinearity of the PEA.

The identified result is shown in Fig. 4(c). It can be found that the steady state of the identified model fits well with the measured experimental data, but the transient part does not fit well. Hence, the unmodeled dynamics caused by the identification process exist and need to be treated as the unknown disturbance as Eq. (12) shows. Therefore, the nominal parameters are $m = 1$, $k = 2.534 \times 10^7$, $b = 5300$. These parameters are used in the ANNFTC as Eqs. (13) and (48) show. Meanwhile, the sensor noise in experiments can also be found in Fig. 4(c). The amplitude of the random noise is generally within ±0.05 μ m. Subsequent closed-loop experiments will verify the controller's robustness against noise of this magnitude.

Furthermore, the hysteresis nonlinearity of the PEA is demonstrated in Fig. 4(d), which depicts the response under a 1 Hz harmonic driving signal with ascending voltage amplitudes (0, 25, 50, 75, and 100 V). It can be observed that the PEA exhibits significant hysteresis loops, and the actual displacement under harmonic excitation deviates from the output predicted by the identified model to be used in controllers. Therefore, the model uncertainty caused by hysteresis nonlinearity must be regarded as an unknown disturbance, as formulated in Eq. (12). This observation underscores the motivation for the control strategy proposed in this study.

5.3. Controller set

The priority of the fixed-time convergence under different initial values of ANNFTC has been sufficiently evaluated and compared with PID, FTC and Finite-time control by simulations in Section 4. Here, to evaluate the tracking performance of the proposed ANNFTC for precision motion control of PEAs in the presence of hysteresis nonlinearity, unmodeled dynamics, and external transient disturbance, ANNFTC is tested by closed-loop experiments in comparison with the FTC and the adaptive FTC (AFTC) in [27]. The controller set for each controller is listed as follows.

5.3.1. FTC

The FTC here is designed with the backstepping method and a stable filter ($1 / (\lambda s+1)$) is applied to the variables v, x_1, and x_d. The overall control law of FTC is applied as follows

$$\begin{aligned} u &= \frac{1}{b}\left(\dot{v}_f + a_2 x_{2f} + a_1 x_{1f} - z_{1f} - z_{2f}/2 + u_{1f} \right), \\ v_f &= -k_1 |z_{1f}|^{\alpha} \mathrm{sign}(z_{1f}) - k_2 |z_{1f}|^{2\beta+1} \mathrm{sign}(z_{1f}) + \dot{x}_{df}, \\ u_{1f} &= -k_3 |z_{2f}|^{\alpha} \mathrm{sign}(z_{2f}) - k_4 |z_{2f}|^{2\beta+1} \mathrm{sign}(z_{2f}). \end{aligned} \tag{58}$$

The filtered variables calculation is done as Eqs. (45)–(47) show.

5.3.2. ANNFTC

The radial basis function network (RBFNN) is adopted to approximate the unknown nonlinearity and dynamics in ANNFTC. From Eq. (24), $\psi(x)$ is the Gaussian function with $\psi(x) = [\psi_1(x), \psi_2(x), \ldots, \psi_M(x)]^T \in \mathbb{R}^M$, and for a M-nodes neural network, the radial basis function of the kth neural network layer is

$$\psi(x)_k = \exp\left(\frac{-\|x - c_k\|^2}{2L} \right), k = 1, 2, \ldots, M. \tag{59}$$

where $c_k = [c_{k,1}, c_{k,2}, \ldots, c_{k,N}]^T \in \mathbb{R}^N$ is the kth neural network layer's center vector, L is the width of the Gaussian function, $M, N \in \mathbb{R}^+$. In this paper, the input vector of the RBFNN is $x = [x_{1f}, x_{2f}]^T$ so that $N = 2$. The overall control law is as Eq. (48) shows.

5.3.3. AFTC in [27]

The AFTC is designed with FTC and neural network (NN) compensation. The difference between the AFTC and the proposed ANNFTC is mainly the adaptive law of the weights of NN. Compared to the adaptive law of AFTC which is designed with asymptotically stable property, the law of ANNFTC can guarantee the fixed-time convergence

of the estimated error of weights. The overall control law of the AFTC is

$$\begin{aligned} u =& \frac{1}{b}\left(\dot{v}_f + a_2 x_{2f} + a_1 x_{1f} - z_{1f} + u_{1f} + \varphi_a \right), \\ v_f =& -k_1 |z_{1f}|^{2p-1} \mathrm{sign}(z_{1f}) - k_2 |z_{1f}|^{2q-1} \mathrm{sign}(z_{1f}) + \dot{x}_{df}, \\ u_{1f} =& -k_3 |z_{2f}|^{2p-1} \mathrm{sign}(z_{2f}) - k_4 |z_{2f}|^{2q-1} \mathrm{sign}(z_{2f}). \\ \varphi_a =& -\frac{1}{2\mu^2} z_{2f} \psi(X)^{\top} \psi(X) \hat{\theta}, X_f = [x_{1f}, x_{2f}], \\ \dot{\hat{\theta}} =& \gamma \left(\frac{1}{2\mu^2} z_{2f}^2 \psi(X)^{\top} \psi(X) - \sigma_1 \hat{\theta} \right). \end{aligned} \tag{60}$$

The NN used in AFTC is also the RBFNN which is the same as the one introduced in Section 5.3.2.

5.4. Parameter tuning

The determination and tuning of the parameters of ANNFTC can be summarized as the following detailed steps:

(1) Tuning the control gain $k_i (i = 1, \ldots, 4)$ and the exponential Values of α and β of the FTC part. The selection of the gain parameter k_i is critical for system performance, as overly small values impede convergence rate while excessively large values induce oscillatory behavior. Since z_1 represents the displacement tracking error and z_2 represents the velocity tracking error, the corresponding gains k_1 and k_3 for z_1 can be tuned to higher values to ensure fast convergence of the tracking error. Conversely, the gains k_2 and k_4 corresponding to z_2 must be constrained to lower magnitudes than k_1 and k_3 to prevent system instability and oscillations driven by amplified velocity error dynamics. Based on extensive simulation and experimental analysis, the following parameter values are determined: k_1 is set to 1000, while k_4 is selected as 0.1, falling within the stable range of (0,0.2] where larger values would trigger undesired oscillatory responses. In comparison, k_2 and k_3 offer greater tuning flexibility within experimental validation, yet remain bounded to avoid interference with the stabilizing effects of k_1 and k_4. Accordingly, k_2 and k_3 are assigned values of 200 and 50, respectively, ensuring balanced dynamic performance without compromising system stability. Based on Eq. (48), α should be selected in the range of (0,1). Hence, α is taken here as 0.5, which is the intermediate value. β can be selected as a positive value. Here, β is selected as 1, which is close to the value of α to balance the effect of the two parameters.

(2) Tuning the parameters of NN: μ, γ, σ_1 and σ_2. Based on Eq. (2), (4), (37) and (40), small values of μ, σ_1 and σ_2 and large value of γ guarantee the estimation accuracy of NN. However, too large γ with too small μ, σ_1 and σ_2 will cause the oscillations. From the simulation test, μ falls within the stable range of [0.45,0.8] and γ should be tuned within [10,150] to avoid oscillations. Here, for pursuing high estimation accuracy of NN, μ is set as 0.5 and γ is set as 100. σ_1 and σ_2 should be tuned in accordance with the value of the real model uncertainty. Other parameters like M, N, and L of the RBFNN are not key to choosing since the weights of RBFNN are tuned online in the control process. The values are selected by experience based on the Refs. [25,26].

(3) After determining the parameters of FTC and NN parts, the rest parameter is the filter parameter λ. The bandwidth of the stable filter (1 / (λ s+1)) is set higher than the maximum tracking frequency to account for the influence of sensor noise and the singularity problem of the calculation of the state variables. From simulation and experimental tests, the cutoff frequency of the filter must be set to at least three times the tracking frequency to avoid affecting tracking accuracy. In the experimental setup, the filter cutoff frequency is set to 50 Hz (higher than three times the frequency of the experimental tracking signals described later) for ANNFTC. The lower cutoff frequency in ANNFTC is necessitated by the structure of the controller: the raw control signal prior to filtering contains high-frequency components originating from the neural network output. This noise makes the signal more susceptible to oscillation, thereby requiring more aggressive filtering to ensure stable operation.

Based on the parameters of ANNFTC, in both FTC and AFTC, the same parameters as those in ANNFTC are preliminarily initialized to be consistent with ANNFTC. Subsequently, considering that the actual experimental platform suffers from the inevitable uncertainties, some parameters of FTC are tuned carefully by an iterative trial and error method to avoid oscillations. Further, since the adaptive law of AFTC differs from ANNFTC, the value of σ_1 and γ are tuned by experiments for the excellent tracking performance of AFTC, while other parameters are kept the same of ANNFTC. This ensures that the comparison of outcomes achieved are suitably fair, as each specified controller has essentially been appropriately and properly tuned. All the parameters used in the experiments are listed below.

Parameters of FTC:

$$\begin{cases} \alpha = 0.5, \beta = 1, \lambda = 0.003183 \\ k_1 = 1000, k_2 = 10, k_3 = 10, k_4 = 0.1 \end{cases} \tag{61}$$

Parameters of ANNFTC:

$$\begin{cases} \alpha = 0.5, \beta = 1, \lambda = 0.003183 \\ k_1 = 1000, k_2 = 200, k_3 = 50, k_4 = 0.1 \\ M = 10, N = 2, L = 0.45, \mu = 0.5, \sigma_1 = 1 \times 10^{-9}, \\ \sigma_2 = 1 \times 10^{-9}, \gamma = 100 \\ c = \begin{bmatrix} -10 & -1 & -0.5 & -0.1 & -0.05 \\ 10 & 1 & 0.5 & 0.1 & 0.05; \\ -200 & -100 & -50 & -1 & -0.5 \\ 100 & 10 & 50 & 10 & 50 \end{bmatrix} \times 0.05 \end{cases} \tag{62}$$

Parameters of AFTC:

$$\begin{cases} p = 0.75, q = 1, \lambda = 0.003183 \\ k_1 = 1000, k_2 = 200, k_3 = 50, k_4 = 0.1 \\ M = 10, N = 2, L = 0.45, \mu = 0.5, \sigma_1 = 10, \gamma = 10 \\ c = \begin{bmatrix} -10 & -1 & -0.5 & -0.1 & -0.05 \\ 10 & 1 & 0.5 & 0.1 & 0.05; \\ -200 & -100 & -50 & -1 & -0.5 \\ 100 & 10 & 50 & 10 & 50 \end{bmatrix} \times 0.05 \end{cases} \tag{63}$$

5.5. Tracking results of ANNFTC

As mentioned above, the design purpose of the ANNFTC is to realize the rapid convergence of tracking error for precision motion tracking under the model uncertainty and external disturbance. To validate the effectiveness of the proposed controller, sinusoidal and triangular trajectories ranging from 1 to 10 Hz and 1 to 9 μ m are used for the references. External disturbances are also added in the experiments. To quantify the tracking errors of different controllers, some error indices are defined as:

$$\begin{aligned} e_{rms} &= \sqrt{\frac{\sum_{i=1}^{n} \left(x(i) - x_d(i)\right)^2}{n}}, \\ e_{nrms} &= \frac{e_{rms}}{A} \times 100\%, \\ e_{max} &= max\left(\left| x(i) - x_d(i) \right| \right), \end{aligned} \tag{64}$$

where e_{rms}, e_{nrms} and e_{max} are the root-mean-square error (RMSE), nominal root-mean-square error (NRMSE) and the maximum tracking error, respectively. x and x_d are the output displacement of PEA and the reference trajectory, i is the sampling number, A is the reference stroke, n is the total number of the data.

5.5.1. Case 1: Results of sinusoidal waves tracking

To test the performance of the proposed ANNFTC in precision motion tracking, sinusoidal waves with different amplitudes and frequencies are set as the reference in this section. The first sinusoidal reference r_1 is: $r_1(t) = 2.5\sin(2\pi t - 0.5\pi) + 3.5$, the second one r_2 is:

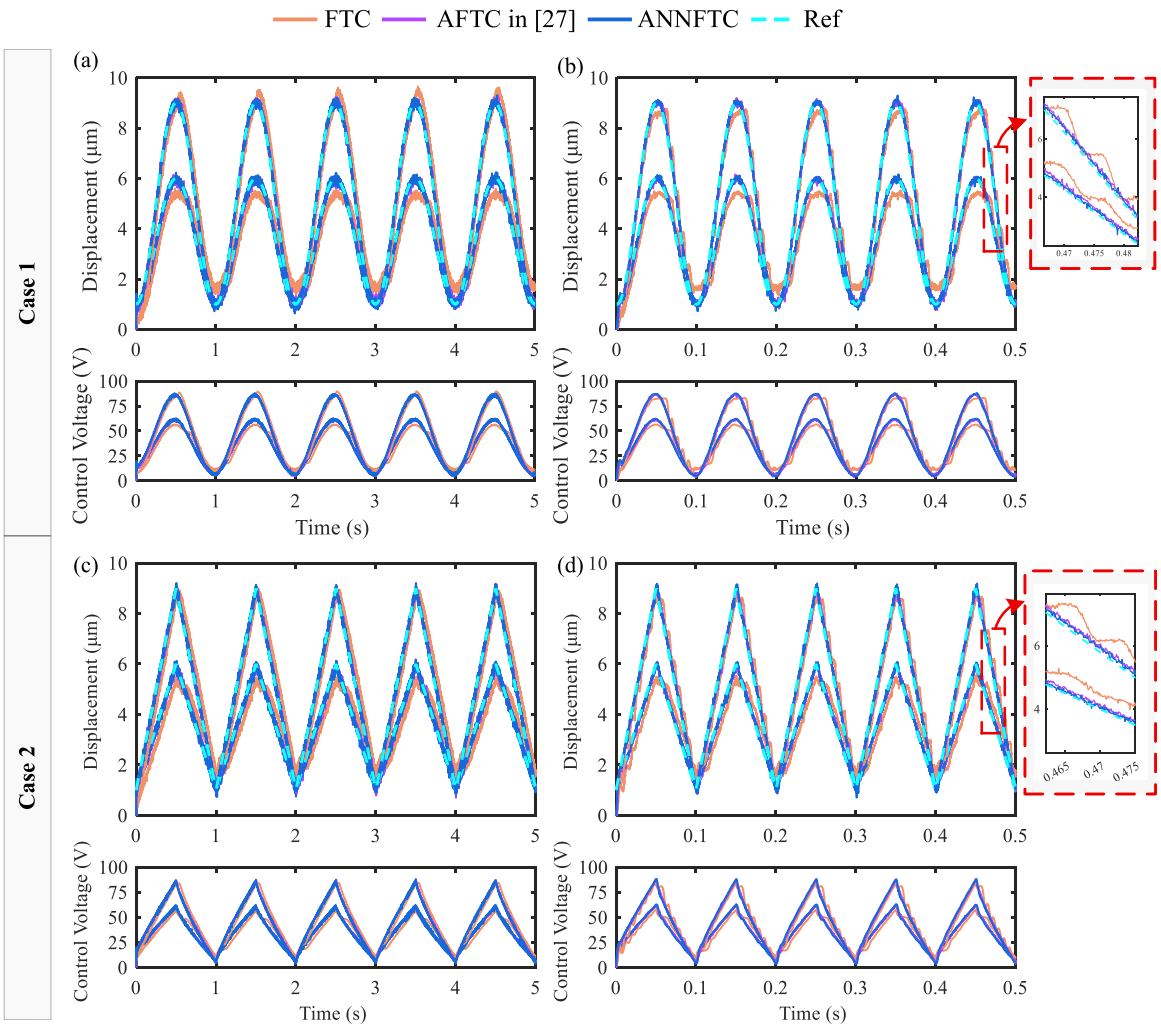

Fig. 5. Results of ANNFTC under Case 1 and Case 2. (a) Tracking results of Case 1: r_1 and r_3. (b) Tracking results of Case 1: r_2 and r_4. (c) Tracking results of Case 2: r_1 and r_3. (d) Tracking results of Case 2: r_2 and r_4.

Table 1
Statistical control results under different tracking references.

Reference trajectories	Statistical data	Sinusoidal tracking			Triangular tracking		
		FTC	ANNFTC (Compared to FTC)	AFTC in [27]	FTC	ANNFTC (Compared to FTC)	AFTC in [27]
r_1	e_{rms} (μm)	0.570	0.067 (↓ 88.3%)	0.097	0.568	0.071(↓ 87.5%)	0.100
	e_{max} (μm)	0.932	0.435	0.477	0.983	0.428	0.458
r_2	e_{rms} (μm)	0.517	0.081 (↓ 84.3%)	0.133	0.515	0.093(↓ 81.9%)	0.134
	e_{max} (μm)	0.885	0.432	0.458	1.292	1.085	0.501
r_3	e_{rms} (μm)	0.629	0.076 (↓ 87.9%)	0.114	0.635	0.082(↓ 87.1%)	0.119
	e_{max} (μm)	1.075	0.353	0.448	1.011	0.394	0.435
r_4	e_{rms} (μm)	0.491	0.105 (↓ 78.6%)	0.163	0.515	0.121(↓ 76.5%)	0.165
	e_{max} (μm)	1.067	0.453	0.560	1.067	0.445	0.486

$r_2(t) = 2.5\sin(20\pi t - 0.5\pi) + 3.5$, the third one r_3 is: $r_3(t) = 4\sin(2\pi t - 0.5\pi) + 5$, the fourth one r_4 is: $r_4(t) = 4\sin(20\pi t - 0.5\pi) + 5$. Overall tracking view and errors of FTC, AFTC and ANNFTC are shown in Fig. 5. It can be found that the proposed ANNFTC can realize the precision tracking of sinusoidal waves within 10 Hz. The RMSE (resp. NRMSE) is below 0.105 μ m (resp. 1.17%). Due to hysteresis and model uncertainty, as Fig. 4(c-d) shows, without NN compensation, the tracking errors of FTC are significantly larger compared to the ones of ANNFTC. This demonstrates the robustness of ANNFTC to model uncertainties, while also highlighting the limitations of FTC and the necessity of ANNFTC. Meanwhile, compared with AFTC, the priority of ANNFTC in tracking performance is not obvious. This is because the AFTC is also integrated with NN compensation. However, compared to AFTC, the superiority of the ANNFTC designed in this paper lies in the fact that the estimation weight errors of the NN also achieve fixed-time convergence. Therefore, ANNFTC exhibits faster convergence speed and greater robustness to transient disturbances compared to AFTC. Hence, the priority of ANNFTC over AFTC will be obvious when the initial value changes and external transient disturbance exists. This case is shown in the following Section 5.5.3.

More detailed data on tracking errors of Case 1 is listed in Table 1. Furthermore, the NN output φ_a and estimated weight $\hat{\theta}$ of ANNFTC under different tracking tests are shown in Fig. 6. It is obvious that φ_a and $\hat{\theta}$ will soon converge and change with the driving period, which matches the periodic characteristics presented by disturbances in tracking periodic signals. The value of the φ_a is as high as 10 to

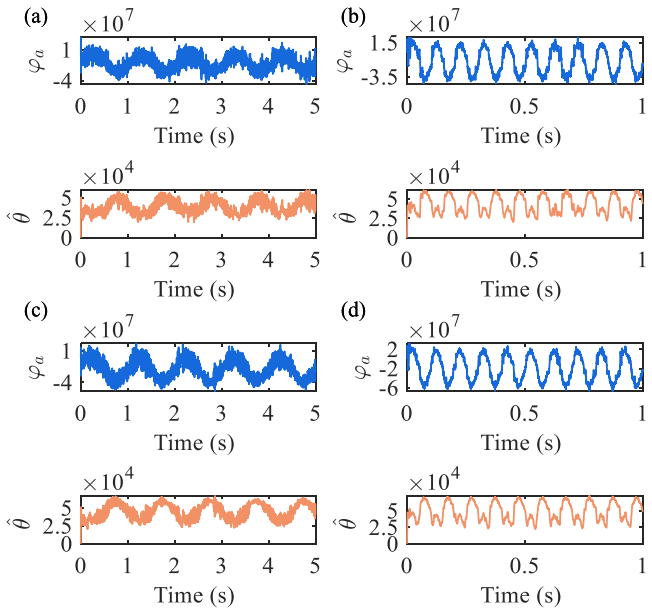

Fig. 6. NN output and convergence results of NN under Case 1. (a) NN results of r_1. (b) NN results of r_2. (c) NN results of r_3. (d) NN results of r_4.

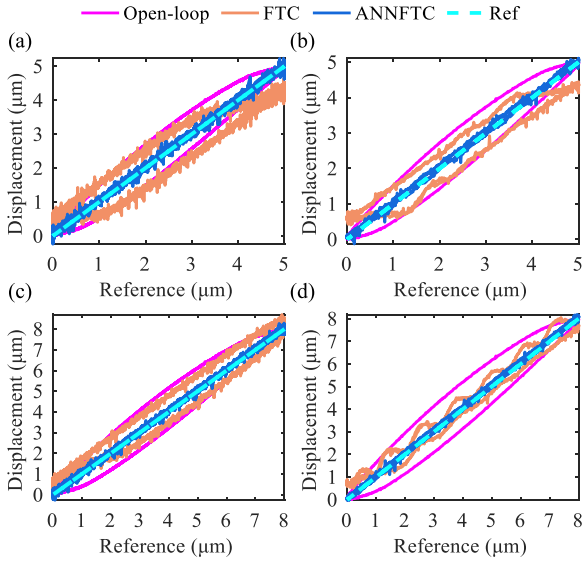

Fig. 7. Hysteresis compensation results of different controllers under Case 1. (a) Results of r_1. (b) Results of r_2. (c) Results of r_3. (d) Results of r_4.

the power 7. This matches the actual disturbance range based on the parameters and model identified shown in Eq. (57). This fact indirectly validates that the inclusion of the neural network (NN) compensates for model uncertainties and hysteresis.

For hysteresis nonlinearity compensation, Fig. 7 presents a comparative evaluation of hysteresis loops under different controllers and tracking references. The open-loop response, acquired in the absence of any controllers, exhibits significant hysteresis. It can be observed that with the compensation of NN, the proposed ANNFTC strategy achieved the ideal Hysteresis compensation, outperforming both the open-loop case and the FTC. In contrast, the FTC alone, while guaranteeing practical fixed-time convergence, fails to effectively mitigate the hysteresis nonlinearity. These results underscore the essential role of the NN component and demonstrate the superiority of the ANNFTC

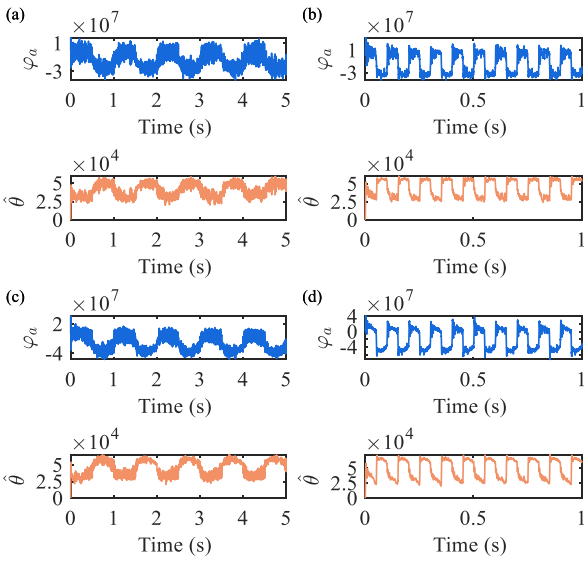

Fig. 8. NN output and convergence results of NN under Case 2. (a) NN results of r_1. (b) NN results of r_2. (c) NN results of r_3. (d) NN results of r_4.

approach in simultaneously satisfying both fixed-time convergence and hysteresis compensation requirements for PEAs.

5.5.2. Case 2: Results of triangular waves tracking

In order to further test the performance of the ANNFTC in tracking multi-harmonic reference, this section is done on the triangular waves tracking. Here, the triangular references r_1 to r_4's amplitudes and periods are in accordance with the aforementioned sinusoidal references r_1 to r_4. The overall tracking view and errors of FTC, AFTC and ANNFTC are shown in Fig. 5. It can also be found that ANNFTC can realize the precision tracking of triangular waves within 10 Hz. Similar conclusions on the convergence independent of the initial states and the NN's convergence and compensation (shown in Fig. 8) can also be drawn. The RMSE (resp. NRMSE) is below 0.121 μ m (resp. 1.34%). More detailed data on tracking errors can be found in Table 1. By comparing the RMSE of the three controllers at different frequencies and amplitudes, it can be observed that, compared to FTC, ANNFTC can reduce the error by at least 76.5%, demonstrating better tracking accuracy. The tracking performances of AFTC and ANNFTC are also similar in this case.

5.5.3. Case 3: Results of disturbance rejection

In order to test the convergence and robustness of the proposed ANNFTC under different initial values and external transient disturbance, an input disturbance is added when tracking a hybrid reference with 2 and 5 Hz. The amplitudes of both the two components are set as 2 μ m. The disturbance is set as an impulse with an amplitude of −20 V, and it occurs at 1.3 s. Furthermore, the initial values of the PEA in this case are set as 0 μ m, 0.5 μ m and 0.8 μ m individually. Results of the overall tracking performance, the maximum error and the recovery time after the disturbance occurrence of the proposed ANNFTC and the AFTC are shown in Fig. 9. Quantitative comparisons among the two controllers can be made from Table 2.

At the beginning of the tracking task, for the three initial conditions, the convergence time of the PEA tracking error under ANNFTC ranges from 2.6 to 2.7 ms, exhibiting close consistency. In contrast, under the AFTC in [27], the convergence time of the tracking error varies with different initial conditions. Furthermore, these durations are generally longer than those of ANNFTC, except when the initial state is set to 0.8 μ m, where the settling time aligns closely with that of ANNFTC.

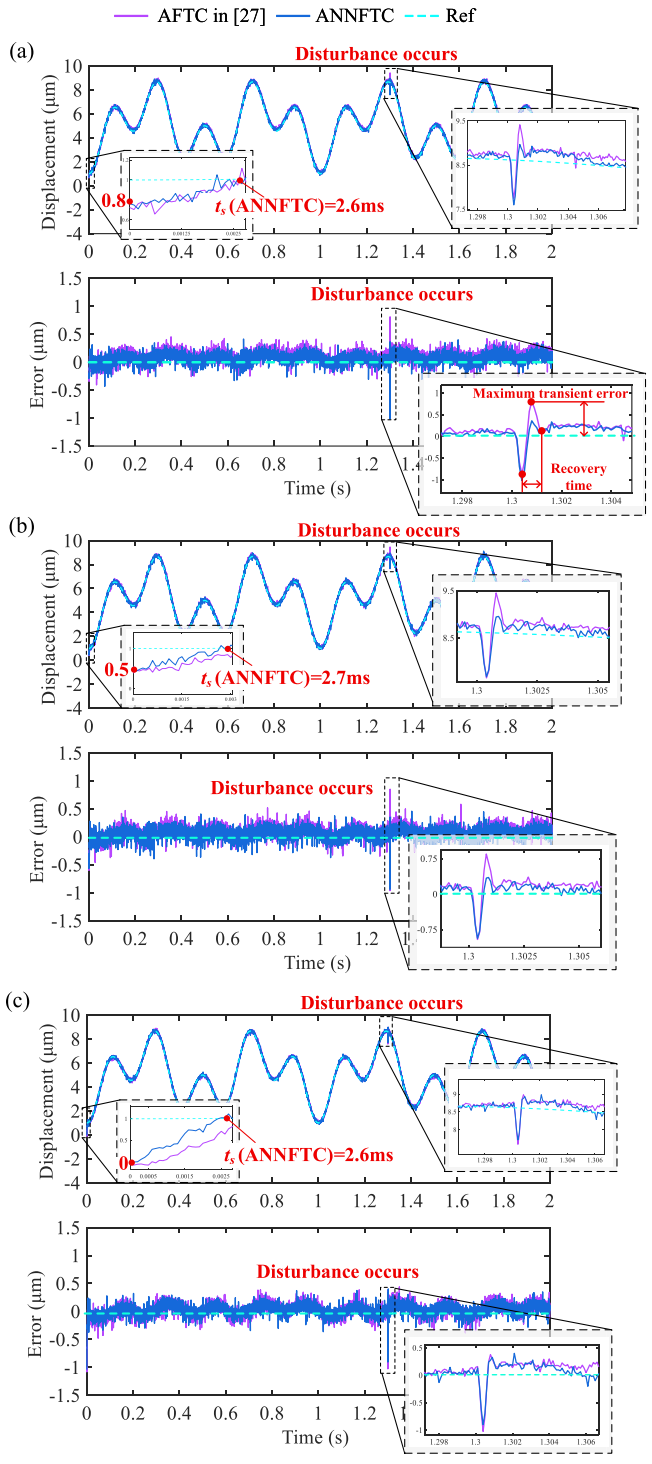

Fig. 9. Results of disturbance rejection for hybrid frequency sinusoidal tracking.

These results highlight the fixed-time convergence capability and the advantage of rapid error convergence offered by the proposed ANNFTC.

Additionally, under the three initial conditions, the maximum tracking error of ANNFTC after a disturbance occurs is comparable to that of the AFTC in [27] when the initial state is zero. However, as the initial condition changes, the maximum tracking error of ANNFTC following a disturbance becomes significantly smaller than that of the AFTC, accompanied by reduced overshoot. This demonstrates the improved motion smoothness of ANNFTC after disturbance occurrence.

Table 2
Statistical control results under disturbance and different initial conditions.

Initial value	Statistical data	Controllers	
		AFTC in [27]	ANNFTC
$x(0) = 0$	Recovery time (ms)	0.7	0.7
	Maximum transient error (μm)	0.38	0.33(↓ 13.2%)
$x(0) = 0.5$	Recovery time (ms)	0.7	0.7
	Maximum transient error (μm)	0.85	0.34(↓ 60.0%)
$x(0) = 0.8$	Recovery time (ms)	0.8	0.7
	Maximum transient error (μm)	0.81	0.36(↓ 55.6%)

Comparing the error convergence capability of the two controllers after a sudden transient external disturbance, the recovery times shown in Fig. 9 indicate that the error convergence times for ANNFTC and AFTC are largely similar for a transient disturbance. The superiority of ANNFTC under input disturbance is primarily reflected in its smaller overshoot following the disturbance.

6. Conclusions

To meet the rapid convergence of tracking error and precision motion tracking of PEAs with inherent nonlinearities and unmodeled dynamics, this paper proposes a novel adaptive neural network fixed-time control (ANNFTC) scheme. The proposed ANNFTC integrates the backstepping method and online neural network compensation, both designed according to the fixed-time stability. Meanwhile, the controller eliminates the need for prior knowledge of hysteresis models or observers, which makes it easy to implement in practice. Experimental results demonstrate ANNFTC's superior tracking performance compared to fixed-time control (FTC) and adaptive FTC (AFTC) in [27], achieving RMSE below 0.121 μ m under 10 Hz and 1–9 μ m triangular references. Meanwhile, under the transient disturbance occurrence, the ANNFTC performs better on the maximum transient error than the AFTC. The significance of this work lies in its dual contribution: (1) providing a theoretically guaranteed adaptive neural network fixed-time control with a novel NN weights adaptive law for PEAs under the existence of model uncertainties through rigorous proof via Lyapunov analysis; and (2) offering a practical control scheme that simplifies implementation by avoiding additional observers or complex parameter tuning with adequate experimental validation. The proposed ANNFTC can be directly extended to other PEA applications, such as nanopositioning stages, microgrippers, or precision surgical devices. Future research directions include: (1) Combining the ANNFTC with the prescribed-time control for PEAs, and (2) Studying the practical application of ANNFTC algorithms in PEAs under varying temperatures and external loads.

CRediT authorship contribution statement

Yunzhi Zhang: Writing – original draft, Visualization, Validation, Methodology, Investigation, Formal analysis, Data curation, Conceptualization. **Zhao Feng:** Writing – review & editing, Supervision, Project administration, Investigation, Funding acquisition. **Jie Ling:** Writing – review & editing, Visualization, Supervision. **Chenyang Ding:** Writing – review & editing, Visualization, Supervision, Resources, Project administration, Funding acquisition.

Declaration of competing interest

The authors declare that they have no known competing financial interests or personal relationships that could have appeared to influence the work reported in this paper.

Acknowledgments

This work was supported in part by the National Key Research Program of China under Grant 2021YFA1200600, the National Natural Science Foundation of China under Grant No. 52405034 and the Hubei Provincial Natural Science Foundation of China under Grant No. 2024AFB126.

References

[1] Amin-Shahidi D, Trumper DL. Design and control of a piezoelectric driven reticle assist device for prevention of reticle slip in lithography systems. Mechatronics 2014;24(6):562–71.
[2] Feng Z, Liang W, Ling J, Xiao X, Tan KK, Lee TH. Precision force tracking control of a surgical device interacting with a deformable membrane. IEEE/ASME Trans Mechatronics 2022;27(6):5327–38.
[3] Ling J, Chen L, Zhang M, Zhu Y. Development of a dual-mode electro-hydrostatic actuator with serial-parallel hybrid configured piezoelectric pumps. Smart Mater Struct 2023;32(2):025011.
[4] Li Q, Ruan Z, Ding C. A new structure and identification method for physical guided neural network based pre-compensator of piezoelectric actuators. Control Eng Pract 2025;162:106365.
[5] Gu G, Zhu L, Su C, Ding H, Fatikow S. Modeling and control of piezo-actuated nanopositioning stages: A survey. IEEE Trans Autom Sci Eng 2014;13(1):313–32.
[6] Al Janaideh M, Al Saaideh M, Rakotondrabe M. On hysteresis modeling of a piezoelectric precise positioning system under variable temperature. Mech Syst Signal Process 2020;145:106880.
[7] Zhang Y, Ling J, Rakotondrabe M, Zhu Y, Wang D. Modeling and feedforward control of hysteresis in piezoelectric actuators considering its rotation and expansion. Mechatronics 2025;110:103354.
[8] Zhou M, Wang Y, Zhang Y, Gao W. Hysteresis inverse compensation-based model reference adaptive control for a piezoelectric micro-positioning platform. Smart Mater Struct 2020;30(1):015019.
[9] Li L, Wang X, Huang W-W, Zhang X, Zhu L. Design of general parametric repetitive control using IIR filter with application to piezo-actuated nanopositioning stages. IEEE Trans Autom Sci Eng 2023;21(2):2102–12.
[10] Sima J, Lai L, Fang Y, Zhu L. Coupled hysteresis and resonance control of three-degree-of-freedom tip-tilt-piston piezoelectric stage. Precis Eng 2024;89:393–407.
[11] Feng Z, Liang W, Ling J, Xiao X, Tan KK, Lee TH. Integral terminal sliding-mode-based adaptive integral backstepping control for precision motion of a piezoelectric ultrasonic motor. Mech Syst Signal Process 2020;144:106856.
[12] Liu Y, Li H, Lu R, Zuo Z, Li X. An overview of finite/fixed-time control and its application in engineering systems. IEEE/CAA J Autom Sin 2022;9(12):2106–20.
[13] Song Y, Ye H, Lewis FL. Prescribed-time control and its latest developments. IEEE Trans Syst Man Cybern: Syst 2023;53(7):4102–16.
[14] Yang H, Ye D. Adaptive fixed-time bipartite tracking consensus control for unknown nonlinear multi-agent systems: An information classification mechanism. Inform Sci 2018;459:238–54.
[15] Xu R, Tian D, Wang Z. Adaptive disturbance observer-based local fixed-time sliding mode control with an improved approach law for motion tracking of piezo-driven microscanning system. IEEE Trans Ind Electron 2024;71(10):12824–34.
[16] Wang Z, Xu R, Tian D. Fast fixed-time adaptive sliding mode control for a piezoelectric-actuated micro-motion stage. Nonlinear Dynam 2025;113(11):13451–66.
[17] Yao Y, Kang Y, Zhao Y, Li P, Tan J. A novel prescribed-time control approach of state-constrained high-order nonlinear systems. IEEE Trans Syst Man Cybern: Syst 2024;54(5):2941–51.
[18] Yao Y, Kang Y, Zhao Y, Li P, Tan J. Prescribed-time output feedback control for cyber–physical systems under output constraints and malicious attacks. IEEE Trans Cybern 2024.
[19] Polyakov A. Nonlinear feedback design for fixed-time stabilization of linear control systems. IEEE Trans Autom Control 2011;57(8):2106–10.
[20] Wang F, Lai G. Fixed-time control design for nonlinear uncertain systems via adaptive method. Systems Control Lett 2020;140:104704.
[21] Liu Z, Zhang O, Gao Y, Zhao Y, Sun Y, Liu J. Adaptive neural network-based fixed-time control for trajectory tracking of robotic systems. IEEE Trans Circuits Syst II: Express Briefs 2022;70(1):241–5.
[22] Liu Z, Zhao Y, Zhang O, Chen W, Wang J, Gao Y, Liu J. A novel faster fixed-time adaptive control for robotic systems with input saturation. IEEE Trans Ind Electron 2023;71(5):5215–23.
[23] Liu Z, Liu J, Zhang O, Zhao Y, Chen W, Gao Y. Adaptive disturbance observer-based fixed-time tracking control for uncertain robotic systems. IEEE Trans Ind Electron 2024;71(11):14823–31.
[24] Zheng D, Pan Y, Guo K, Yu H. Identification and control of nonlinear systems using neural networks: A singularity-free approach. IEEE Trans Neural Netw Learn Syst 2019;30(9):2696–706.
[25] Ling J, Feng Z, Zheng D, Yang J, Yu H, Xiao X. Robust adaptive motion tracking of piezoelectric actuated stages using online neural-network-based sliding mode control. Mech Syst Signal Process 2021;150:107235.
[26] Ling J, Feng Z, Chen L, Zhu Y, Pan Y. Neural network-based iterative learning control of a piezo-driven nanopositioning stage. Precis Eng 2023;81:112–23.
[27] Ba D, Li Y-X, Tong S. Fixed-time adaptive neural tracking control for a class of uncertain nonstrict nonlinear systems. Neurocomputing 2019;363:273–80.
[28] Sun W, Diao S, Su S-F, Sun Z-Y. Fixed-time adaptive neural network control for nonlinear systems with input saturation. IEEE Trans Neural Netw Learn Syst 2021;34(4):1911–20.
[29] Mei Y, Wang J, Park JH, Shi K, Shen H. Adaptive fixed-time control for nonlinear systems against time-varying actuator faults. Nonlinear Dynam 2022;107(4):3629–40.
[30] Yuan X, Chen B, Lin C. Neural adaptive fixed-time control for nonlinear systems with full-state constraints. IEEE Trans Cybern 2021;53(5):3048–59.
[31] Qian C, Lin W. Non-Lipschitz continuous stabilizers for nonlinear systems with uncontrollable unstable linearization. Systems Control Lett 2001;42(3):185–200.
[32] Zhu Z, Xia Y, Fu M. Attitude stabilization of rigid spacecraft with finite-time convergence. Internat J Robust Nonlinear Control 2011;21(6):686–702.
[33] Xie S, Chen Q. Adaptive nonsingular predefined-time control for attitude stabilization of rigid spacecrafts. IEEE Trans Circuits Syst II: Express Briefs 2021;69(1):189–93.